

1 **Connection between sea surface anomalies and atmospheric**
2 **quasi-stationary waves**

3 G. Wolf*

4 *Department of Meteorology, University of Reading, Reading, United Kingdom.*

5 *National Centre for Atmospheric Sciences, University of Reading, Reading, United Kingdom*

6 A. Czaja

7 *Imperial College, London, United Kingdom*

8 D.J. Brayshaw and N.P. Klingaman

9 *Department of Meteorology, University of Reading, Reading, United Kingdom.*

10 *National Centre for Atmospheric Sciences, University of Reading, Reading, United Kingdom*

11 **Corresponding author address:* G. Wolf, Department of Meteorology, Earley Gate, University of
12 Reading, P.O. Box 243, Reading, Berkshire RG6 6BB, United Kingdom.

13 E-mail: g.a.wolf@reading.ac.uk

ABSTRACT

14 Large scale, quasi-stationary atmospheric waves (QSWs) are known to be
15 strongly connected with extreme events and general weather conditions. Yet,
16 despite their importance, there is still a lack of understanding about what
17 drives variability in QSW. This study is a step towards this goal, and identi-
18 fies three statistically significant connections between QSWs and sea surface
19 anomalies (temperature and ice cover) by applying a maximum covariance
20 analysis technique to reanalysis data (1979-2015). The two most dominant
21 connections are linked to the El Niño Southern Oscillation and the North At-
22 lantic Oscillation. They confirm the expected relationship between QSWs and
23 anomalous surface conditions in the tropical Pacific and the North Atlantic,
24 but they cannot be used to infer a driving mechanism or [predictability \[previ-](#)
25 [ously: predictive skill\]](#) from the sea surface temperature or the sea ice cover
26 to the QSW. The third connection, in contrast, occurs between late winter
27 to early spring Atlantic sea ice concentrations and anomalous QSW patterns
28 in the [following \[previously written in italic\]](#) late summer to early autumn.
29 This new finding offers a pathway for possible long term predictability of late
30 summer QSW occurrence.

31 **1. Introduction**

32 Weather in mid-latitudes is typically associated with synoptic scale transient cyclones and anti-
33 cyclones, but occasionally more persistent weather regimes on scales of several days to about two
34 weeks can be observed (Horel 1985). These persistent weather regimes are often associated with
35 blocking highs at the jet exit regions (Masato et al. 2014) as part of a longitudinally extended
36 “quasi-stationary” wave (QSW, e.g. Nakamura et al. 1997; Wolf et al. 2018b).

37 QSWs are important because of their strong influence on weather and their link to extreme
38 events. Periods with increased QSW activity tend to be associated with more extremes, whereas
39 the absence of QSWs is linked to “near-average” weather (Screen and Simmonds 2014; Wolf
40 et al. 2018b). This connection between extreme events and mid-latitude wave patterns has been
41 suggested in several case studies (e.g. Petoukhov et al. 2016; Fragkoulidis et al. 2018) although
42 it is difficult to infer a general relationship from case studies alone (Screen and Simmonds 2013;
43 Petoukhov et al. 2013). Wolf et al. (2018b) showed the most dominant Northern Hemisphere QSW
44 patterns and the QSW patterns most relevant for European temperature extremes and anomalies
45 events and temperature anomalies, with strong correlations also to seasonal averages.

46 Despite the importance of QSWs, there is still a lack of understanding about possible large
47 scale drivers of the QSW variability. Most promising is the strong suggestion from literature that
48 large-scale [low-frequency variability patterns \[previously: climate patterns\]](#), like El Niño Southern
49 Oscillation (ENSO) or North Atlantic Oscillation (NAO), can be linked to QSW patterns. Further,
50 sea surface temperature (SST) and sea ice concentration (SIC) anomalies seem to be linked to jet
51 variability and therefore also to QSW patterns.

52 ENSO may control the spatial and temporal variability of QSW activity of a full season, leading
53 to extreme events in North America (Trenberth and Guillemot 1996; Pan et al. 1999). It is well

54 known that a tropical heating source can lead to stationary anomalies in the general circulation
55 (Gill 1980), but its effects on non-stationary waves in mid-latitudes and teleconnections to extreme
56 events are less clear. Souders et al. (2014) have shown the anomalous wave pattern occurrence for
57 transient waves during La Niña and El Niño. Furthermore, the impact of ENSO on the Atlantic is
58 weaker and modulated by the Atlantic multidecadal oscillation, such that during its negative phase
59 the ENSO teleconnection is more apparent (Rodríguez-Fonseca et al. 2016).

60 In Europe, the NAO has a strong influence on temperature anomalies (Pozo-Vázquez et al. 2001)
61 and even strong droughts can be associated with the NAO phase (López-Moreno and Vicente-
62 Serrano 2008). To some extent, the NAO can be related to processes outside the Atlantic region,
63 connected by the presence of a wave. Jiang et al. (2017) showed that the Madden-Julian Oscil-
64 lation influences the behavior and persistence of NAO positive and negative phases. Feldstein
65 (2003) investigated the time evolution of the NAO associated with transients and QSWs, showing
66 a connection between the positive NAO and a preceding Pacific wavetrain.

67 The connection between sea ice anomalies and circulation changes are of particular importance,
68 because the persistence of sea ice anomalies makes them a possible source of seasonal to inter-
69 annual predictability. [There is progress in understanding the connection between a changing cli-
70 mate and the tropospheric and stratospheric circulation response \(e.g. review of Screen et al.
71 2018\), but the \[previously: . The\] impact of sea ice on mid-latitude waves in a changing climate is
72 still uncertain and \[included\] widely discussed.](#) Some studies conclude that stronger sea ice loss
73 leads to decreased baroclinicity which can lead to more persistent wave patterns (e.g. Overland
74 et al. 2016), whereas other studies link reduced sea ice with fewer planetary waves due to a weak-
75 ening of the baroclinic-eddy wave source (e.g. Smith et al. 2017). These discrepancies highlight
76 the necessity to further investigate and understand the atmospheric wave response to variabil-
77 ity in sea surface temperatures and sea ice. It is difficult to isolate the atmospheric response to

78 changes in sea ice due to the many other influences on the atmospheric circulation, as well as a
79 low signal-to-noise-ratio (Screen et al. 2014). Regarding this aspect, Luo et al. (2019) highlighted
80 the importance of the weakened north-south gradient of background potential vorticity (PV) over
81 Eurasia for Ural blocking and cold winters in East Asia. The weakened PV gradient was linked
82 therein to a warming climate and reduced sea ice. The cold events, however, can also occur during
83 a weakened PV gradient even without negative sea ice anomalies as a result of mid-latitude cold
84 anomalies, but still only if there is blocking. Such dependencies could be responsible for some of
85 the above-mentioned discrepancies and the difficulties to come to a clear conclusion [additional
86 text included].

87 Several studies link specific local changes in sea ice to impacts on the atmospheric circulation.
88 Wu et al. (2013) showed that above average winter sea ice concentrations west of Greenland can
89 lead to Atlantic SST anomalies persisting into spring, which feed back on the atmospheric sum-
90 mer circulation in northern Eurasia. Hall et al. (2017) showed that the Atlantic May SST tripole,
91 showing increased correlations with SST anomalies of the preceding months, can be associated
92 with the Atlantic jet speed in summer, while sea ice anomalies could also be related to a latitudinal
93 shift in the jet location. Petrie et al. (2015) found the Labrador sea ice concentration to be rele-
94 vant for the jet strength over North America, which affects north-western Europe via downstream
95 developing wave packets. Cause and effect between QSWs and sea ice anomalies is not always
96 obvious and should be considered with caution (Simmonds and Govekar 2014). For example, Sato
97 et al. (2014) linked anomalous sea ice retreats in the Barents-Kara sea to a shift in the Gulf Stream
98 front, leading to an atmospheric wave response with a teleconnection to the Arctic. These studies
99 further motivate investigating the connection between sea ice anomalies and QSW patterns.

100 The remainder of this paper is organized as follows. Section 2 presents the data and methods
101 used to calculate QSWs and to relate them to surface ocean anomalies (sea surface temperature

102 and sea ice concentrations). Results obtained by the application of the statistical method described
103 in section 2 are presented in section 3. Section 4 analyses the connection between late winter/early
104 spring sea surface anomalies and the associated QSW patterns in late summer/early autumn and
105 its possible physical connections. The key conclusions of this paper are summarized in section 5.

106 2. Data and methods

107 ERA-Interim reanalysis (Dee et al. 2011) is used for all meteorological quantities on a longitude-
108 latitude grid with $0.75^\circ \times 0.75^\circ$ resolution. The data are linearly detrended at each gridpoint over
109 1979 to 2015 for each season individually. This procedure allows us to focus on the intra-annual
110 connections between variables, without the effect of long term trends.

111 To identify the envelope field of the quasi-stationary waves (QSW) at 300 hPa we use the method
112 of Wolf et al. (2018b). The envelope field of the QSW is a phase independent, non-negative
113 measure of the waviness of the anomalous meridional wind, v' , in the zonal direction. We refer to
114 this envelope field as the amplitude of the QSW. The anomalous meridional wind is calculated as
115 $v' = \tilde{v} - \bar{\tilde{v}}$, where \tilde{v} is the 15-day lowpass filtered meridional wind - to remove faster transients -
116 and $\bar{\tilde{v}}$ is the daily climatology, to which we also applied a 15 day lowpass filter.

117 From this anomalous wind field, the phase-independent amplitude of the wave is calculated
118 using the method of Zimin et al. (2003). For this method a wavenumber range must be chosen,
119 which is assumed to represent the spatial scale of the waves of interest. In this study a wavenumber
120 range of about 4 to 8 in mid-latitudes is chosen, but instead of using a fixed wavenumber range,
121 a latitude-dependent wavenumber range is used, with a cosine decay towards higher latitudes,
122 following the maxima of the power spectra of the anomalous meridional wind v' (Wolf et al.

123 2018b, details therein)¹. The cosine weighting essentially leads to a latitude-independence of the
124 range of wavelengths, rather than of the wavenumbers. An advantage of the applied QSW method,
125 compared to other commonly used methods (such as Screen and Simmonds 2014; Kornhuber et al.
126 2017), is that it is a positive and phase independent measure of the wave packet in longitude-
127 latitude fields for one time-step. This allows to represent the spatial pattern of the investigated
128 wave packets and the application of time averages without having to deal with the problems of
129 phase cancellation (as it would be the case for time averages of anomalies of geopotential height
130 or meridional wind).

131 To identify statistical connections between QSWs and SST and SIC we apply a maximum co-
132 variance (MC) analysis between those variables, as described in Czaja and Frankignoul (2002).
133 The MC is calculated between monthly averaged anomaly fields. The anomalies are calculated as
134 the deviation from the climatological mean of the specific month. The regions used for the MC
135 analysis of the two variables are not necessarily the same and will be defined later. This method
136 identifies the modes that maximize the covariance between two possibly different variables, sim-
137 ilar to empirical orthogonal functions, which identify the modes that maximize the variance of
138 one variable in the underlying data. For investigating the covariance between different seasons,
139 monthly anomalies within each season are used. The term “season” refers to a period of any three
140 consecutive months. Introducing further a time lag for one of the variables identifies potentially
141 causal relationships. To give similar weight to each season, the anomalies are further normalized
142 by the standard deviation of the specific variables in the specific season. To identify the relevance
143 of specific modes, a Monte Carlo approach is applied to determine if the modes are statistically
144 significant. The method is therefore a purely statistical approach to connect variables in the under-

¹The data for the 12 hourly envelope fields of the quasi-stationary waves between [1 June 1979](#) and [31 August 2015](#) [previously: [01.06.1979](#) and [31.08.2015](#)], are available at the Centre for Environmental Data Analysis (Wolf et al. 2018a).

145 lying data; it does not include any information about the nature of possible physical connections.
146 For the MC analysis of two variables in different seasons, the Monte Carlo approach repeats the
147 MC calculation 1000 times (if not stated otherwise) by holding the first variable fixed, but ran-
148 domly permutating the years for the second variable. The permutation is, however, only applied to
149 each season as a whole. This means that consecutive months within one season in the MC analysis
150 are preserved in the Monte Carlo approach; only the years are shuffled. It is important to realize
151 that the results of the MC analysis cannot by themselves be used as proof of causality, even when
152 strong lead/lag relationships are found between variables. Instead, MCA analysis is used here to
153 identify potential causal patterns in order to stimulate the further investigations required to identify
154 physical causal processes.

155 To represent sea surface anomalies, we combine the fields of SST and SIC into one matrix, be-
156 fore applying the MC analysis. To do so, both fields are normalized by their seasonal standard
157 deviation, using all gridpoints at which anomalies could be observed in the dataset for the asso-
158 ciated season. For SIC, this includes all gridpoints inside the maximum areal extent of SIC in
159 the dataset. The combined matrix is created by concatenating both normalized matrices along the
160 latitude dimension. The MC analysis then proceeds as usual by assuming that the combined field
161 represents one variable. In the following, we will refer to the combined field as SSTSIC. The MC
162 patterns using either SST or SIC individually are qualitatively very similar. In case of a difference
163 to the combined SSTSIC, this will be highlighted in the text. Note that the technique is linear so
164 that the signs of patterns shown in the figures below can be reversed (the relative signs between
165 QSW and SSTSIC remaining unchanged).

166 The values for the global pattern indices used in this study, namely the North Atlantic Os-
167 cillation (NAO) and the El Niño Southern Oscillation in the Niño 3.4 region (Niño 3.4), are

168 retrieved from the CPC database of the National Oceanic and Atmospheric Administration
169 (<http://www.cpc.ncep.noaa.gov>).

170 **3. Connection between ocean anomalies and QSWs**

171 In this section we identify connections between anomalous QSW amplitudes and anomalies in
172 SSTSIC using monthly averages. We do this by applying the MC analysis between those two
173 variables, as described in section 2, for various regions and with lags between -6 and $+9$ months
174 (QSW leads surface variables at negative lags). Results are shown in Fig. 1a (extended Northern
175 Hemisphere SSTSIC anomalies) and Fig. 2a (Atlantic SSTSIC anomalies). These figures display
176 in colour the squared covariance of the leading MC mode between QSW and SSTSIC as a function
177 of season and time lag, following Czaja and Frankignoul (2002, their Fig. 1). For example in
178 Fig. 1a, large squared covariances are found when SSTSIC is taken in NDJ (x-axis) and QSW two
179 months later (JFM, white rectangle highlighted). It is worth noting that the largest synchronous
180 values occur during the colder seasons. Statistical significance is indicated by the green plusses
181 in these plots while the contours display the correlation coefficient between large scale modes of
182 climate variability and the QSW leading mode timeseries. Application of this procedure reveals
183 three statistically significant connections which are discussed in the following three subsections.

184 *a. Connection between QSWs and El Niño Southern Oscillation*

185 High covariances for the first MC mode between extended Northern Hemisphere SSTSIC (20°S
186 to 85°N) and extratropical Northern Hemisphere QSWs (30°N to 85°N) in Fig. 1a identify strong
187 lead/lag connections between those variables for all seasons. The connection for all seasons can
188 be understood by a persistent SSTSIC anomaly from the warmer seasons into the colder seasons
189 (strong covariances along the diagonal line from top left to bottom right in Fig. 1a) with strong

190 QSW anomalies manifesting only during the colder seasons. Due to the persistence of these
191 increased covariances, the covariances during summer with large positive lags are also potentially
192 physically meaningful, although not statistically significant. Since the statistically significant co-
193 variances (green dots and plusses) occur in an area of the plot which does show high correlations
194 between the time series of the principal component of QSW and the Niño 3.4 index (black con-
195 tours in Fig. 1a), we can associate this connection to El Niño Southern Oscillation (ENSO). Since
196 this connection represents the clear first mode in the MC analysis, ENSO can be identified, on a
197 hemispheric scale, as the dominant oceanic anomaly associated with QSW variability.

198 The diagonal tilting of the statistically significant covariances in Fig. 1a along a straight line
199 indicates that this connection exists for QSW patterns mainly from DJF to FMA. Due to the con-
200 nection to ENSO with the strongest anomalies in the tropical Pacific, it is not surprising that this
201 specific connection is dominated by the SST contribution and cannot be reproduced by using SIC
202 only (not shown).

203 The associated latitude-longitude pattern of the MC mode between SSTSIC in NDJ and QSW
204 amplitudes in JFM (lag of +2 months, white box in Fig. 1a) shows increased QSW amplitudes
205 over the Pacific, North America and the subtropical Atlantic and decreased QSW amplitudes over
206 Europe and the high-latitude North Atlantic during La Niña (Fig. 1b, continuous and dashed con-
207 tours, respectively - the La Niña state is clearly seen in the SST anomaly pattern shown in colour
208 in Fig. 1b). Due to the linearity of the MC analysis, the exact opposite is true for El Niño (flipped
209 signs for both SSTSIC and QSW). The patterns for the statistically significant covariances at pos-
210 itive lags are very similar, whereas for negative lags this is less clear (not shown here). Due to
211 the long persistence of SST anomalies during ENSO phases of either sign and the statistical sig-
212 nificance occurring at both positive and negative lags, it is impossible to deduce a direct forcing
213 of QSW variability by the SST pattern in Fig. 1. Modeling work is necessary to understand how

214 such strong covariances come about, perhaps through an atmospheric bridge (Lau and Nath 1994;
215 Alexander et al. 2002). The connection between the ENSO SST pattern and QSW therefore sug-
216 gests predictive skill for the QSW insofar as the ENSO SST pattern in itself tends to be strongly
217 persistent (thus a month with warm SSTs tends to be followed by another warm SST month, con-
218 sistent with similar QSW patterns being observed in both). This should not, however, be taken
219 to imply a direct causal connection between ENSO SSTs and remote QSW anomalies at some
220 later time. A seasonal forecast model that skillfully predicted the persistence for ENSO might also
221 skillfully predict the preferred QSW pattern, but such an investigation is outside the scope of this
222 paper.

223 *b. Connection between QSWs and North Atlantic Oscillation*

224 Using again the same region for the QSW amplitudes (30°N to 85°N), but reducing the region
225 for the SSTSIC to the North Atlantic north of 20°N (80°W to 40°E), the first MC mode shows
226 strong covariances associated with negative lags (Fig. 2a, i.e. QSW leads SSTSIC). These covari-
227 ances are associated with the NAO (blue contour lines). The statistically significant covariances at
228 negative lags suggest that the NAO-related SSTSIC pattern is reflecting a forcing of the ocean by
229 the atmosphere, consistent with previous studies (e.g. Czaja and Frankignoul 2002; Visbeck et al.
230 2003). For the phase shown in Fig.2b, it consists of a tripolar SST anomaly, with colder conditions
231 along the separated Gulf Stream sandwiched between anomalously warm conditions to the north
232 and south (colours). The SIC pattern is, in response to a negative NAO phase, less sea ice in the
233 Labrador sea (green contours) and more sea ice in the Greenland-Barents Sea (magenta contours).

234 The associated wave pattern (Fig. 2b, based on the lags/month highlighted by white box at
235 negative lags in Fig. 2a) represents a reduction of wave amplitude over 30°N and an enhancement
236 poleward of 50°N. It was shown to be associated with cold temperatures at 850 hPa in Central

237 Europe (Wolf et al. 2018b), agreeing with previous results for temperature anomalies associated
238 with the negative phase of the NAO (Pozo-Vázquez et al. 2001). The shift between the strongest
239 covariances and highest correlation in Fig. 2a is the result of an evolving QSW pattern, from mid-
240 latitudes towards high latitudes and a further shift from the Pacific towards the Atlantic (not shown
241 here). Only the pattern at the later stage of this evolving QSW signal (Fig. 2b) is strongly correlated
242 with the NAO, which is the reason for the reduced correlations occurring for the preceding seasons.
243 However, the associated SST pattern is consistent and shows for all negative lags the typical NAO-
244 like Atlantic SST-tripole (as the one in Fig. 2b) and therefore are those QSW patterns also expected
245 to be associated with the NAO. As for the connection to ENSO, this connection is also associated
246 dominantly with QSW anomalies during winter and the adjacent months. In winter, ENSO and
247 NAO show strong correlations with the first three EOFs of Northern hemispheric QSW amplitudes
248 (Wolf et al. 2018b), which highlights again the importance of these two QSW patterns.

249 *c. Connection between QSWs and North Atlantic high latitude surface ocean anomalies*

250 Besides the dominant two connections with ENSO or the NAO, we identified a third significant
251 connection through MC analysis between late winter to early spring SSTSIC and late summer to
252 early autumn QSW amplitudes (second white box in Fig. 2a, i.e. SSTSIC in FMA leads QSW by
253 about 5 months).

254 The associated latitude-longitude QSW pattern in JAS shows increased mid-latitude and de-
255 creased high latitude QSW amplitudes (Fig. 2c), covarying with the SST tripole and SIC anomalies
256 described above. That is, we find a very similar SSTSIC pattern but associated at lag +5 months
257 with a generally opposing QSW pattern than found at lag -1 month (i.e., the signs of the anomaly
258 in the high and mid-latitude regions are reversed). Note that the lags of +4 and +6 months show
259 a consistent QSW pattern (not shown). In addition, the same statistically significant pattern can

260 be reproduced using only SST or only SIC for the MC analysis, instead of the combined SSTSIC
261 field (not shown here).

262 The pattern of increased mid-latitude QSW amplitudes in summer (Fig. 2c) is linked to strong
263 lower troposphere temperature anomalies of either sign (but mainly warm anomalies) over Central
264 Europe (Wolf et al. 2018b). QSW composites associated with extreme warm anomalies in the
265 same region showed a very similar wave pattern. Further, cold anomalies in Central Europe were
266 associated with preceding increased high latitude QSW activity. This suggests that the QSW
267 patterns, related to European temperature anomalies in summer could be linked to Atlantic SSTSIC
268 anomalies in late winter to early spring.

269 A further separation of the SSTSIC region into northern and southern parts (20°N to 60°N and
270 60°N to 85°N) reveals that the MC analysis for the northern part leads to statistically significant
271 covariances, whereas MC analysis for the southern part does not (not shown here; see section 4
272 below for more sensitivity tests of the MC analysis). The associated longitude-latitude patterns
273 for the northern part are very similar to the ones using the full Atlantic region (20°N to 85°N).
274 This suggests the importance of high latitude sea surface anomalies for this connection, but the
275 associated longitude-latitude patterns for the southern part show similarities to the ones for the
276 northern part, at least for lags of +5 and +6 months, meaning that the southern part is not nec-
277 essarily irrelevant for this teleconnection. The role of the SIC in this connection is investigated
278 further in section 4.

279 To check the robustness of this connection between FMA SSTSIC and subsequent JAS QSW
280 amplitudes, we calculated composite FMA SSTSIC anomalies for the 8 JAS seasons with the
281 strongest QSW anomalies in mid- (225°W to 45°E, 40°N to 60°N: 1987, 1985, 1998, 1981, 2003,
282 2007, 1986 and 1995) and high latitudes (North of 65°N: 1984, 1995, 1993, 1979, 2008, 1991,
283 1983 and 2004), where the years given in brackets are ordered by their intensity, starting with

284 the highest intensity. The resulting SSTSIC patterns are very similar to the one given in Fig. 2c
285 (not shown). The results are not sensitive to the number of seasons used for the composite. This
286 supports the hypothesis of a connection between SSTSIC in FMA and QSW amplitudes in the
287 following JAS. We now briefly investigate possible physical mechanisms for this connection.

288 **4. Possible physical links for the inter-seasonal ocean and QSW connection**

289 In the previous section we have already shown the importance of the high-latitude Atlantic for
290 the connection between late winter/early spring SSTSIC anomalies and late summer/early autumn
291 QSW amplitude anomalies. Using only SIC for the MC analysis leads to more statistically signif-
292 icant signals of the same patterns for neighbouring seasons with similar lags (Fig. S1), additional
293 to the previously found statistically significant signal at a lag of +5 months for FMA by using
294 SST only or SSTSIC (Fig. 2a). From this we can hypothesize that SIC is the main contributor
295 to this connection. Such SIC anomalies, if persistent enough, could interact with the large scale
296 atmospheric circulation by modifying the baroclinicity, acting on similar sub-annual timescales as
297 in previous studies (e.g. Wu et al. 2013). We possibly see an atmospheric response in summer
298 and not spring, because of the importance of the jet location relative to the region of the modified
299 baroclinicity. The center (defined by the peak intensity) of the lower tropospheric jet at 850 hPa
300 in the Atlantic jet entry region may still be too far south in April to June (climatological value at
301 42°N, between 60°W and 30°W), whereas in July to September it shifts northward (climatological
302 value at 49°N). This means that the change in baroclinicity by the higher-latitude ocean anoma-
303 lies close to the Labrador Sea in April to June do not align well with the jet position in the West
304 Atlantic, which therefore does not optimally contribute as a baroclinic energy source for further
305 wave amplification. This could change, once the climatological jet location moves towards higher
306 latitudes in the following months. As discussed in the introduction, this source of energy could

307 be a relevant mechanism for wave amplification (e.g. Smith et al. 2017). How this interaction
308 works clearly needs further investigation but the statistical result reported here appears robust. We
309 proceed below to further analysis of the empirical relationship captured in Fig. 2c.

310 To interact with the late summer atmospheric circulation, the late winter SIC anomalies must
311 be persistent enough. To check the persistence of these SIC anomalies, we calculate a lag com-
312 posite of area-averaged SST and SIC anomalies in the Greenland-Barents Sea (0°E to 60°E , 50°N
313 to 80°N) and Labrador Sea (70°W to 50°W , 50°N to 65°N) for the 8 seasons with the strongest
314 positive and negative SIC differences between those two regions in FMA (Fig. 3a). As a reminder,
315 those regions are chosen to cover the relevant SIC anomalies for the investigated connection in
316 this section (see Fig. 2b and c). We refer to this difference as I_{diff} . Positive values indicate more
317 anomalous sea ice in the Greenland-Barents Sea than in the Labrador Sea. All composite anoma-
318 lies (SST and SIC) for positive I_{diff} (solid lines) and negative I_{diff} (dashed lines) show the same sign
319 until JAS. This persistence is insensitive to the number of seasons used for the composite. If these
320 anomalies are optimally aligned to interact with the wave guide in summer, this could cause the
321 anomalous QSW patterns in summer.

322 Similar to the previous test of robustness, we calculate the QSW patterns in JAS for the years
323 with the strongest positive (1979, 2011, 2010, 1981, 1998, 1987, 2004 and 2003) and negative
324 values (1984, 1993, 1983, 1990, 1992, 1991, 1995 and 2014) for I_{diff} . As expected from the results
325 of the MC analysis, the composite for the years with negative I_{diff} values leads to anomalously strong
326 high latitude QSW amplitudes (Fig. 3b), exceeding the 99th percentile (white dots). The composite
327 for the years with positive I_{diff} values leads to anomalous strong and statistically significant mid-
328 latitude QSW amplitudes (Fig. 3c), although there is a gap of increased QSW amplitudes over
329 North America. But overall, the sign of I_{diff} clearly leads to a separation of the QSW patterns with

330 strong values at high or mid-latitudes. The qualitative results are insensitive to the exact choice of
331 the regions used to calculate I_{diff} , as long as they capture the dipole character of this anomaly.

332 Comparing the SSTSIC in Fig. 2b and 2c reveals very similar patterns. This suggests that the
333 NAO, which is strongly associated with the QSW and SST pattern of Fig. 2b, represents the com-
334 mon feature behind both connections (the ones shown in Fig. 2b and Fig. 2c). The associated
335 SSTSIC pattern found for both connections therefore appears to link the two atmospheric anoma-
336 lies in autumn/winter and the following summer/autumn. This would mean that the autumn/winter
337 QSW pattern leads to a specific late winter/spring SSTSIC pattern which further leads to a specific
338 QSW pattern in late summer/early autumn. In the following we will provide further support for
339 this hypothesis. First for the connection between winter NAO index and the following late sum-
340 mer/early autumn QSW anomalies. For this connection we obtain a linear correlation of -0.42
341 between mid-latitude (225°W to 45°E and 40°N to 60°N) averaged QSW amplitudes in JAS and
342 the averaged NAO value in the preceding DJF (Fig. S2a), whereas strong high-latitude (north of
343 65°N) averaged QSW amplitudes in JAS seem to occur mainly after a positive NAO in the pre-
344 ceding DJF (Fig. S2b). Second, if the above hypothesis is true, one can possibly expect increased
345 covariances between similar QSW patterns in autumn/winter and the following summer/autumn.
346 To test this we repeated the MC analysis of Fig. 2a between extratropical Northern Hemisphere
347 QSW amplitudes and QSW amplitudes limited to the Atlantic basin (instead of SSTSIC limited
348 to the Atlantic basin). The QSW amplitudes in the second region are restricted to the Atlantic
349 basin, because of the known strong connection between Atlantic QSW anomalies and the NAO
350 (Wolf et al. 2018b, or Fig. 2a and 2b herein). This MC analysis indeed shows a statistically signif-
351 icant connection between autumn to winter Atlantic QSW amplitudes and Northern Hemisphere
352 QSW amplitudes with about a $+7$ month lag, which further show increased correlations with NAO
353 (Fig. S3). Because of the strong atmospheric internal variability and its nonlinear behaviour, the

354 presented linear statistical method does not prove this hypothesis, but supports the potential for
355 recurrent interactions between QSWs, SST and SIC anomalies between autumn to winter and late
356 summer to early autumn. To clarify the details of these recurrent interactions, further analysis is
357 necessary.

358 **5. Conclusion and discussion**

359 In a previous study (Wolf et al. 2018b) we showed the connection between QSWs and European
360 weather and extreme events and identified the main modes of QSW variability. We highlighted
361 therein the importance of better understanding the physical mechanisms underlying these QSW
362 patterns and their variability. This analysis represents the first step towards this goal by investigat-
363 ing the link between surface ocean anomalies and QSW amplitudes with lags of several months.
364 Therefore, we use the MC analysis as a powerful tool to identify statistical connections between
365 different variables, as done in previous studies (e.g. Czaja and Frankignoul 2002; Frankignoul
366 et al. 2014).

367 We identified three statistical significant connections between sea surface anomalies and anoma-
368 lous QSW amplitudes. The two most dominant connections occur during the colder seasons (late
369 autumn, winter, early spring) and can be related to ENSO and NAO. These global pattern indices
370 are not only linked to strong temperature anomalies and extreme events (e.g. Pan et al. 1999;
371 Pozo-Vázquez et al. 2001; López-Moreno and Vicente-Serrano 2008), but they can also be asso-
372 ciated with some predictability (Latif et al. 1998; Scaife et al. 2014). It is therefore important to
373 understand the evolution of the associated QSW patterns, which are more directly linked to the as-
374 sociated weather and therefore can help to get a deeper understanding of the evolution of extremes
375 or why predictability increases in remote regions. [This is no contradiction with the previous state-
376 ment that our results for the ENSO connection cannot be used to infer predictability for the QSWs.](#)

377 The results from the applied statistical method could only be used to highlight the general con-
378 nection between the SST associated with ENSO and mid-latitude QSWs. The QSW pattern itself
379 indicates possible teleconnection regions, but to understand the details of the teleconnections or
380 the time evolution and frequency of the QSWs during an ENSO event, further analysis beyond this
381 monthly lagged analysis is needed. During La Niña we identified an increase in QSW amplitudes
382 over the North Pacific and North America, reaching downstream into the subtropical Atlantic to-
383 wards the Mediterranean, whereas over the high-latitude North Atlantic and Europe a decrease
384 in QSW amplitudes can be observed. For the Atlantic SST tripole, associated with the negative
385 NAO phase, QSW amplitudes show increased values at high latitudes with a maximum over the
386 Atlantic and a slight decrease along the subtropical Asian jet. This connection exists for QSW
387 amplitudes with negative lags in the MC analysis, suggesting the SST tripole to be an imprint of
388 the preceding atmospheric flow pattern. This dominant atmosphere-driving-ocean relationship is
389 in agreement with previous studies (e.g. Czaja and Frankignoul 2002; Visbeck et al. 2003). These
390 QSW patterns, associated with NAO and ENSO, explain a large contribution of the overall QSW
391 variability during the cold season. The focus in that [previously: this] paragraph, concerning the
392 global pattern indices, was towards La Niña and the negative NAO phase. Due to the linearity of
393 the MC analysis, the exact opposite is true for El Niño or the positive NAO (reversed signs for
394 both SSTSIC and QSW, relative signs remain unchanged).

395 The third statistical significant connection between those two variables occurs between FMA
396 Atlantic high latitude sea surface anomalies and JAS extratropical Northern Hemisphere QSW
397 anomalies. We identified the SIC as the main contributor to this connection. The large lag of
398 about +5 months can possibly be attributed to the persistence of the associated SIC pattern. We
399 showed that for years with a strong anomaly of such a SIC pattern in FMA, this anomaly persists
400 into JAS. Interacting with the general circulation, these sea ice anomalies could be responsible for

401 the QSW response in the following late summer/early autumn. The reason why this interaction is
402 not apparent during late spring/early summer could be that the locations between the baroclinic
403 modified region by the SIC or associated SST anomalies and the wave guide for the QSWs are not
404 optimally aligned. How this interaction works in detail needs further investigation.

405 Our results about the FMA SSTSIC anomalies show strong similarities with the findings of
406 Frankignoul et al. (2014), in which they showed that the Atlantic SIC anomalies in the Labrador
407 sea and Greenland-Barents Sea (they refer to it as “seesaw” pattern) during late winter/early spring
408 can be associated to preceding NAO anomalies and which by itself leads to a NAO-like pattern
409 of opposite polarity about 6 weeks later. This suggests the same underlying driving mechanism
410 between winter NAO and FMA SSTSIC anomalies, but distinct to the analysis of Frankignoul
411 et al. (2014), we identified a longer lag connection between their “seesaw” pattern and upper
412 tropospheric QSWs in JAS. In agreement with our findings, they also identified SIC anomalies as
413 the main contributor to this connection. They further discussed that including the North Pacific SIC
414 dipole pattern of negative and positive anomalies in the Bering and Okhotsk Sea, which appears
415 also in our findings (see Fig. 2c), increases the statistical significance.

416 To test the robustness of the results, we included a composite analysis, showing the same sea
417 surface or QSW patterns as for the linear MC analysis by applying a ± 5 months lag to each of the
418 composited variables separately. This further increases the confidence in the findings of the applied
419 statistical analysis. Due to the findings of the connection between NAO and QSW anomalies
420 in autumn to winter, the connection between winter NAO and FMA SSTSIC anomalies and the
421 connection between FMA SSTSIC anomalies and JAS QSW anomalies, we hypothesized that a
422 connection between autumn to winter QSWs and QSWs in the following JAS may be apparent.
423 Repeating the MC analysis for QSW amplitudes between different seasons does indeed show
424 increased covariances, supporting this hypothesis.

425 These results are all based on the first MC modes for the different regions or variables, to high-
426 light the most dominant and robust signals. Higher MC modes also include some statistically
427 significant signals, but those are fewer and less coherent. The second MC modes show mainly
428 two statistically significant signals. For SSTSIC in the extratropical Northern Hemisphere (first
429 mode given in Fig. 1a) the area of the statistically significant covariances is very similar to the one
430 found for negative lags in Fig. 2a, also with increased correlations with the winter NAO index,
431 meaning that the second MC mode for extratropical Northern Hemisphere SSTSIC describes the
432 same signal as the first MC mode for SSTSIC in the Atlantic region. The second MC mode for
433 SSTSIC in the Atlantic shows statistically significant signals in spring to summer, with a lag of
434 about +4 months. The SSTSIC signal is represented again by the previously discussed NAO-like
435 imprint. The associated QSW patterns are also partly very similar to the signal found for FMA
436 with a +5 lag, suggesting that the previously identified SSTSIC not only appears in late winter, but
437 also into spring and summer. The patterns are less coherent, however, and besides the very similar
438 QSW pattern we can also identify a similar SSTSIC pattern, but which is associated with a east-
439 west dipole in QSW amplitudes, with positive anomalies towards Europe and negative over North
440 America for a negative NAO. This second mode could explain the gap of increased mid-latitude
441 QSW amplitudes in the composite study (Fig. 3c).

442 In this paper we were able to link some important QSW patterns to surface ocean anomalies.
443 Due to the more direct link of the QSW patterns to the associated weather, compared to the use of
444 global pattern indices, their consideration can be helpful in the understanding and interpretation
445 of specific teleconnection patterns. We further demonstrated the relevance of SIC anomalies on
446 the QSW patterns of following seasons, which can be very helpful for long term predictability of
447 large scale weather conditions or the occurrence of extremes.

448 *Acknowledgments.* We acknowledge funding from the Natural Environment Research Council
449 (NERC) for the ODYSEA project (grant number: NE/M006085/1). Nicholas P. Klingaman was
450 funded by a NERC Independent Research Fellowship (NE/L010976/1).

451 **References**

452 Alexander, M. A., I. Blad, M. Newman, J. R. Lanzante, N.-C. Lau, and J. D. Scott, 2002: The
453 atmospheric bridge: The influence of enso teleconnections on airsea interaction over the global
454 oceans. *Journal of Climate*, **15** (16), 2205–2231, doi:10.1175/1520-0442(2002)015<2205:
455 TABTIO>2.0.CO;2.

456 Czaja, A., and C. Frankignoul, 2002: Observed impact of atlantic sst anomalies on the north
457 atlantic oscillation. *J. Climate*, **15** (6), 606–623, doi:10.1175/1520-0442(2002)015<0606:
458 OIOASA>2.0.CO;2.

459 Dee, D. P., and Coauthors, 2011: The era-interim reanalysis: configuration and performance of
460 the data assimilation system. *Quart. J. Roy. Meteor. Soc.*, **137** (656, A), 553–597, doi:10.1002/
461 qj.828.

462 Feldstein, S. B., 2003: The dynamics of nao teleconnection pattern growth and decay. *Quart. J.*
463 *Roy. Meteor. Soc.*, **129** (589), 901–924, doi:10.1256/qj.02.76.

464 Fragkoulidis, G., V. Wirth, P. Bossmann, and A. H. Fink, 2018: Linking northern hemisphere
465 temperature extremes to rossby wave packets. *Quart. J. Roy. Meteor. Soc.*, **144** (711), 553–566,
466 doi:10.1002/qj.3228.

467 Frankignoul, C., N. Sennéchaël, and P. Cauchy, 2014: Observed atmospheric response to
468 cold season sea ice variability in the arctic. *J. Climate*, **27** (3), 1243–1254, doi:10.1175/
469 JCLI-D-13-00189.1.

- 470 Gill, A. E., 1980: Some simple solutions for heatinduced tropical circulation. *Quart. J. Roy. Meteor. Soc.*, **106 (449)**, 447–462, doi:10.1002/qj.49710644905.
- 471
- 472 Hall, R. J., J. M. Jones, E. Hanna, A. A. Scaife, and R. Erdélyi, 2017: Drivers and potential
473 predictability of summer time north atlantic polar front jet variability. *Climate Dyn.*, **48 (11)**,
474 3869–3887, doi:10.1007/s00382-016-3307-0.
- 475 Horel, J. D., 1985: Persistence of the 500 mb height field during northern hemisphere winter. *Mon.*
476 *Wea. Rev.*, **113 (11)**, 2030–2042, doi:10.1175/1520-0493(1985)113<2030:POTMHF>2.0.CO;2.
- 477 Jiang, Z., S. B. Feldstein, and S. Lee, 2017: The relationship between the maddenjulian oscillation
478 and the north atlantic oscillation. *Quart. J. Roy. Meteor. Soc.*, **143 (702)**, 240–250, doi:10.1002/
479 qj.2917.
- 480 Kornhuber, K., V. Petoukhov, D. Karoly, S. Petri, S. Rahmstorf, and D. Coumou, 2017: Summer-
481 time planetary wave resonance in the northern and southern hemispheres. *J. Climate*, **30 (16)**,
482 6133–6150, doi:10.1175/JCLI-D-16-0703.1.
- 483 Latif, M., and Coauthors, 1998: A review of the predictability and prediction of enso. *Journal of*
484 *Geophysical Research: Oceans*, **103 (C7)**, 14 375–14 393, doi:10.1029/97JC03413.
- 485 Lau, N.-C., and M. J. Nath, 1994: A modeling study of the relative roles of tropical and extratrop-
486 ical sst anomalies in the variability of the global atmosphere-ocean system. *Journal of Climate*,
487 **7 (8)**, 1184–1207, doi:10.1175/1520-0442(1994)007<1184:AMSOTR>2.0.CO;2.
- 488 López-Moreno, J. I., and S. M. Vicente-Serrano, 2008: Positive and negative phases of the win-
489 tertime north atlantic oscillation and drought occurrence over europe: A multitemporal-scale
490 approach. *J. Climate*, **21 (6)**, 1220–1243, doi:10.1175/2007JCLI1739.1.

- 491 Luo, D., X. Chen, J. Overland, I. Simmonds, Y. Wu, and P. Zhang, 2019: Weakened potential
492 vorticity barrier linked to recent winter arctic sea ice loss and midlatitude cold extremes. *Journal*
493 *of Climate*, **32** (14), 4235–4261, doi:10.1175/JCLI-D-18-0449.1.
- 494 Masato, G., T. Woollings, and B. J. Hoskins, 2014: Structure and impact of atmospheric blocking
495 over the euro-atlantic region in present-day and future simulations. *Geophys. Res. Lett.*, **41** (3),
496 1051–1058, doi:10.1002/2013GL058570.
- 497 Nakamura, H., M. Nakamura, and J. Anderson, 1997: The role of high- and low-frequency dynam-
498 ics in blocking formation. *Mon. Wea. Rev.*, **125** (9), 2074–2093, doi:10.1175/1520-0493(1997)
499 125<2074:TROHAL>2.0.CO;2.
- 500 North, G., T. Bell, R. Cahalan, and F. Moeng, 1982: Sampling errors in the estimation of em-
501 pirical orthogonal functions. *Mon. Wea. Rev.*, **110** (7), 699–706, doi:10.1175/1520-0493(1982)
502 110<0699:SEITEO>2.0.CO;2.
- 503 Overland, J., and Coauthors, 2016: Nonlinear response of mid-latitude weather to the changing
504 arctic. *Nature Climate Change*, **6**, 992–999, doi:10.1038/NCLIMATE3121.
- 505 Pan, Z., M. Segal, R. Arritt, T. Chen, and S. Weng, 1999: A method for simulating effects of
506 quasi-stationary wave anomalies on regional climate. *J. Climate*, **12** (5, 1), 1336–1343, doi:
507 10.1175/1520-0442(1999)012<1336:AMFSEO>2.0.CO;2.
- 508 Petoukhov, V., S. Petri, S. Rahmstorf, D. Coumou, K. Kornhuber, and H. J. Schellnhuber, 2016:
509 Role of quasiresonant planetary wave dynamics in recent boreal spring-to-autumn extreme
510 events. *Proc. Natl. Acad. Sci. (USA)*, **113** (25), 6862–6867, doi:10.1073/pnas.1606300113.

511 Petoukhov, V., S. Rahmstorf, S. Petri, and H. J. Schellnhuber, 2013: Reply to screen and
512 simmonds: From means to mechanisms. *Proceedings of the National Academy of Sciences*,
513 **110 (26)**, E2328–E2328, doi:10.1073/pnas.1305595110.

514 Petrie, R. E., L. C. Shaffrey, and R. T. Sutton, 2015: Atmospheric response in summer linked to
515 recent arctic sea ice loss. *Quart. J. Roy. Meteor. Soc.*, **141 (691)**, 2070–2076, doi:10.1002/qj.
516 2502.

517 Pozo-Vázquez, D., M. J. Esteban-Parra, F. S. Rodrigo, and Y. Castro-Díez, 2001: A study of nao
518 variability and its possible non-linear influences on european surface temperature. *Climate Dyn.*,
519 **17 (9)**, 701–715, doi:10.1007/s003820000137.

520 Rodríguez-Fonseca, B., and Coauthors, 2016: A review of enso influence on the north atlantic. a
521 non-stationary signal. *Atmosphere*, **7 (7)**, doi:10.3390/atmos7070087.

522 Sato, K., J. Inoue, and M. Watanabe, 2014: Influence of the gulf stream on the barents sea ice re-
523 treat and eurasian coldness during early winter. *Environmental Research Letters*, **9 (8)**, 084 009,
524 doi:10.1088/1748-9326/9/8/084009.

525 Scaife, A. A., and Coauthors, 2014: Skillful longrange prediction of european and north american
526 winters. *Geophys. Res. Lett.*, **41 (7)**, 2514–2519, doi:10.1002/2014GL059637.

527 Screen, J. A., T. J. Bracegirdle, and I. Simmonds, 2018: Polar climate change as manifest
528 in atmospheric circulation. *Current Climate Change Reports*, **4 (4)**, 383–395, doi:10.1007/
529 s40641-018-0111-4.

530 Screen, J. A., C. Deser, I. Simmonds, and R. Tomas, 2014: Atmospheric impacts of arctic sea-
531 ice loss, 1979–2009: separating forced change from atmospheric internal variability. *Climate*
532 *Dynamics*, **43 (1)**, 333–344”, doi:10.1007/s00382-013-1830-9.

533 Screen, J. A., and I. Simmonds, 2013: Caution needed when linking weather extremes to amplified
534 planetary waves. *Proceedings of the National Academy of Sciences*, **110** (26), E2327–E2327,
535 doi:10.1073/pnas.1304867110.

536 Screen, J. A., and I. Simmonds, 2014: Amplified mid-latitude planetary waves favour particular
537 regional weather extremes. *Nature Climate Change*, **4** (8), 704–709, doi:10.1038/nclimate2271.

538 Simmonds, I., and P. D. Govekar, 2014: What are the physical links between arctic sea ice loss
539 and eurasian winter climate? *Environmental Research Letters*, **9** (10), 101 003, doi:10.1088/
540 1748-9326/9/10/101003.

541 Smith, D. M., N. J. Dunstone, A. A. Scaife, E. K. Fiedler, D. Copsey, and S. C. Hardiman, 2017:
542 Atmospheric response to arctic and antarctic sea ice: The importance of oceanatmosphere cou-
543 pling and the background state. *J. Climate*, **30** (12), 4547–4565, doi:10.1175/JCLI-D-16-0564.
544 1.

545 Souders, M. B., B. A. Colle, and E. K. M. Chang, 2014: The climatology and characteristics
546 of rossby wave packets using a feature-based tracking technique. *Mon. Wea. Rev.*, **142** (10),
547 3528–3548, doi:10.1175/MWR-D-13-00371.1.

548 Trenberth, K., and C. Guillemot, 1996: Physical processes involved in the 1988 drought and 1993
549 floods in north america. *J. Climate*, **9** (6), 1288–1298, doi:10.1175/1520-0442(1996)009<1288:
550 PPIITD>2.0.CO;2.

551 Visbeck, M., E. P. Chassignet, R. G. Curry, T. L. Delworth, R. R. Dickson, and G. Krahnmann,
552 2003: *The Ocean's Response to North Atlantic Oscillation Variability*, 113–145. American Geo-
553 physical Union (AGU), doi:10.1029/134GM06.

- 554 Wolf, G., D. J. Brayshaw, N. P. Klingaman, and A. Czaja, 2018a: Envelope field of northern
555 hemispheric upper tropospheric (300 hpa) quasi-stationary waves (june 1979 to august 2015).
556 *Centre for Environmental Data Analysis*, doi:10.5285/c0c7998800414e46b6823dc75751bb4c.
- 557 Wolf, G., D. J. Brayshaw, N. P. Klingaman, and A. Czaja, 2018b: Quasi-stationary waves and
558 their impact on european weather and extreme events. *Quart. J. Roy. Meteor. Soc.*, **144** (717),
559 2431–2448, doi:10.1002/qj.3310.
- 560 Wu, B., R. Zhang, R. D’Arrigo, and J. Su, 2013: On the relationship between winter sea ice
561 and summer atmospheric circulation over eurasia. *J. Climate*, **26** (15), 5523–5536, doi:10.1175/
562 JCLI-D-12-00524.1.
- 563 Zimin, A. V., I. Szunyogh, D. Patil, B. R. Hunt, and E. Ott, 2003: Extracting envelopes of rossby
564 wave packets. *Mon. Wea. Rev.*, **131** (5), 1011–1017, doi:10.1175/1520-0493(2003)131<1011:
565 EEORWP>2.0.CO;2.

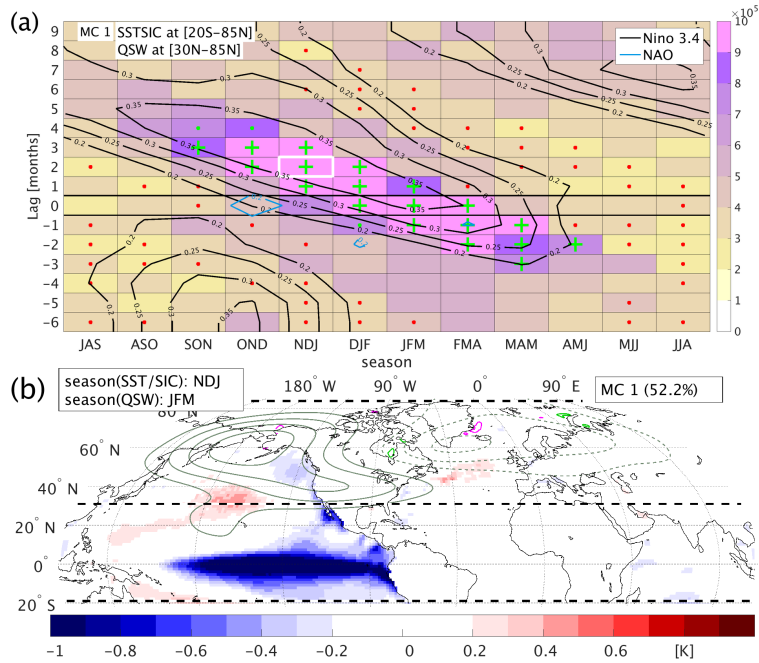
566 **6. Figures**

567 **LIST OF FIGURES**

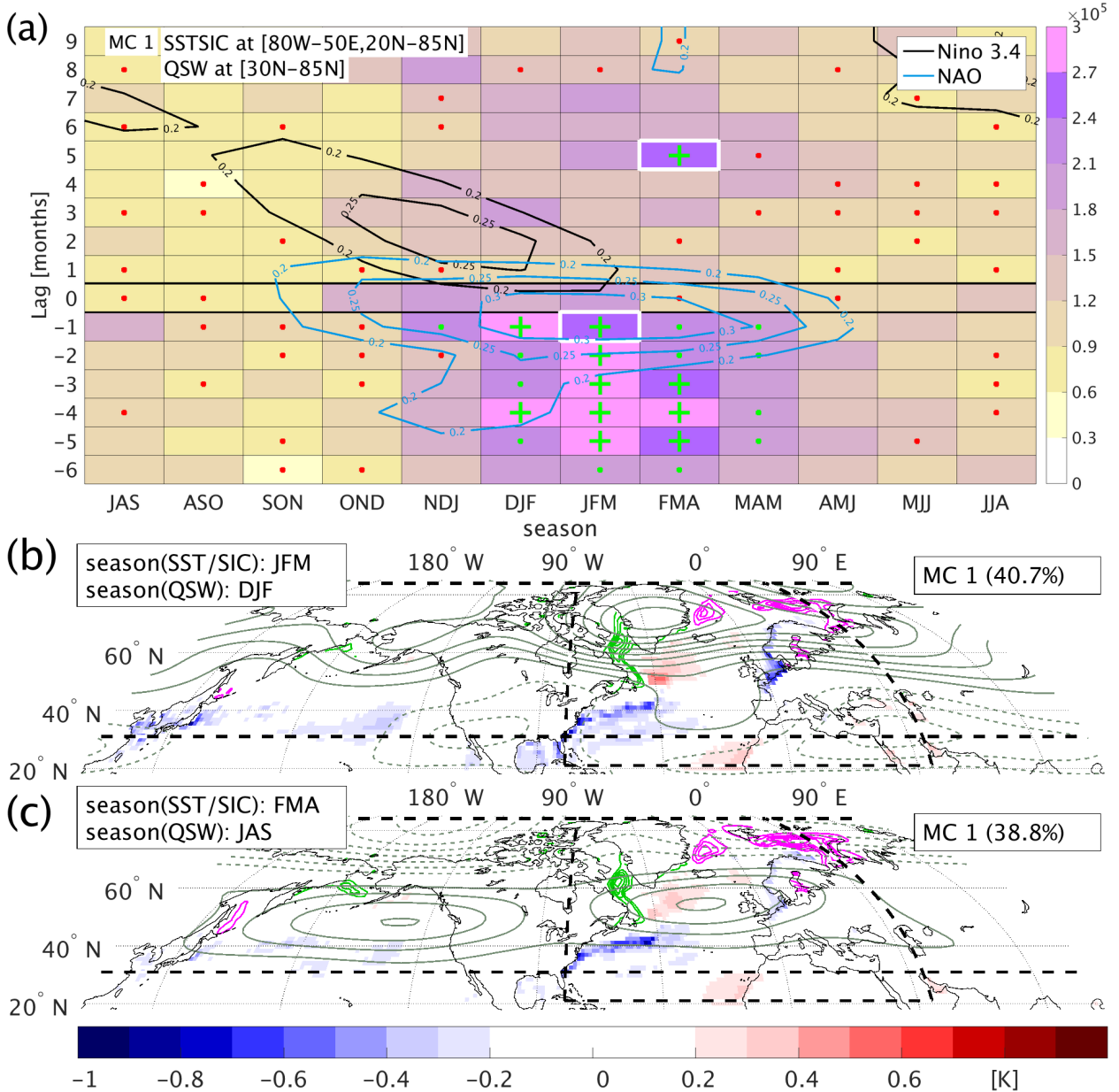
568 **Fig. 1.** Panel (a) shows the first MC mode for the lagged covariance matrix between extended
 569 Northern Hemisphere (20°S to 85°N) SSTSIC and extratropical Northern Hemisphere
 570 (30°N to 85°N) QSW anomalies. Shading represents covariance between associated anom-
 571 alies, weighted by their respective seasonal standard deviation. Seasons for the SSTSIC fields
 572 are given in panel (a) on the x-axis and are represented by the initial letters of the associ-
 573 ated months. For the seasonally averaged QSW amplitudes a lag of -6 to +9 months is
 574 applied (given on the y-axis); positive lags therefore mean that the SSTSIC is leading QSW.
 575 [excluded (description of stat. sign. in the method section): Statistical significance is cal-
 576 culated by using a Monte Carlo approach, repeating the analysis 1000 times with the same
 577 seasons and lags, but randomly choosing years for the QSWs.] Green plusses (dots) show
 578 statistical significant covariances based on 95th (90th) percentile. Red dots show those in-
 579 stances when the MC mode is not separable from the following mode, following the rule of
 580 thumb of North et al. (1982). Additional contour lines represent correlations between one
 581 of two global pattern indices (Niño 3.4 in black and NAO in blue) and the lagged QSW MC
 582 mode.
 583 Panel (b) shows the associated latitude-longitude pattern for the box, marked by the white
 584 edges in panel (a), for NDJ SSTSIC and JFM QSW (lag of +2 months). Boundaries for
 585 the regions used in the MC analysis are given by the black dashed lines. Shading shows
 586 anomalies of SST. Gray solid (dashed) contour lines show positive (negative) anomalies of
 587 QSW amplitude, spaced every 0.5 m/s omitting the zero contour line. Magenta (positive
 588 values) and green (negative values) contour lines show anomalies in SIC, spaced every 0.04
 589 omitting the zero contour line. All variables shown are calculated via the projection of this
 590 variable onto the timeseries of the first principal component. 28

591 **Fig. 2.** First MC mode between Atlantic (80°W to 50°E and 20°N to 85°N) SSTSIC and extrat-
 592 ropical Northern Hemisphere (30°N to 85°N) lagged QSW anomalies (boundaries of these
 593 regions shown by black dashed lines in panel (b) and (c)). Panel (b) and (c) show the asso-
 594 ciated latitude-longitude pattern for the boxes, marked by the white edges in panel (a), for
 595 JFM SSTSIC and DJF QSW (panel b, lag -1 month) and for FMA SSTSIC and JAS QSW
 596 (panel c, lag +5 months). Gray solid (dashed) contour lines show positive (negative) anom-
 597 alies of QSW amplitude, spaced every 0.25 m/s omitting the zero contour line. Description
 598 for all other shadings, contours, etc. are the same as in Fig. 1. 29

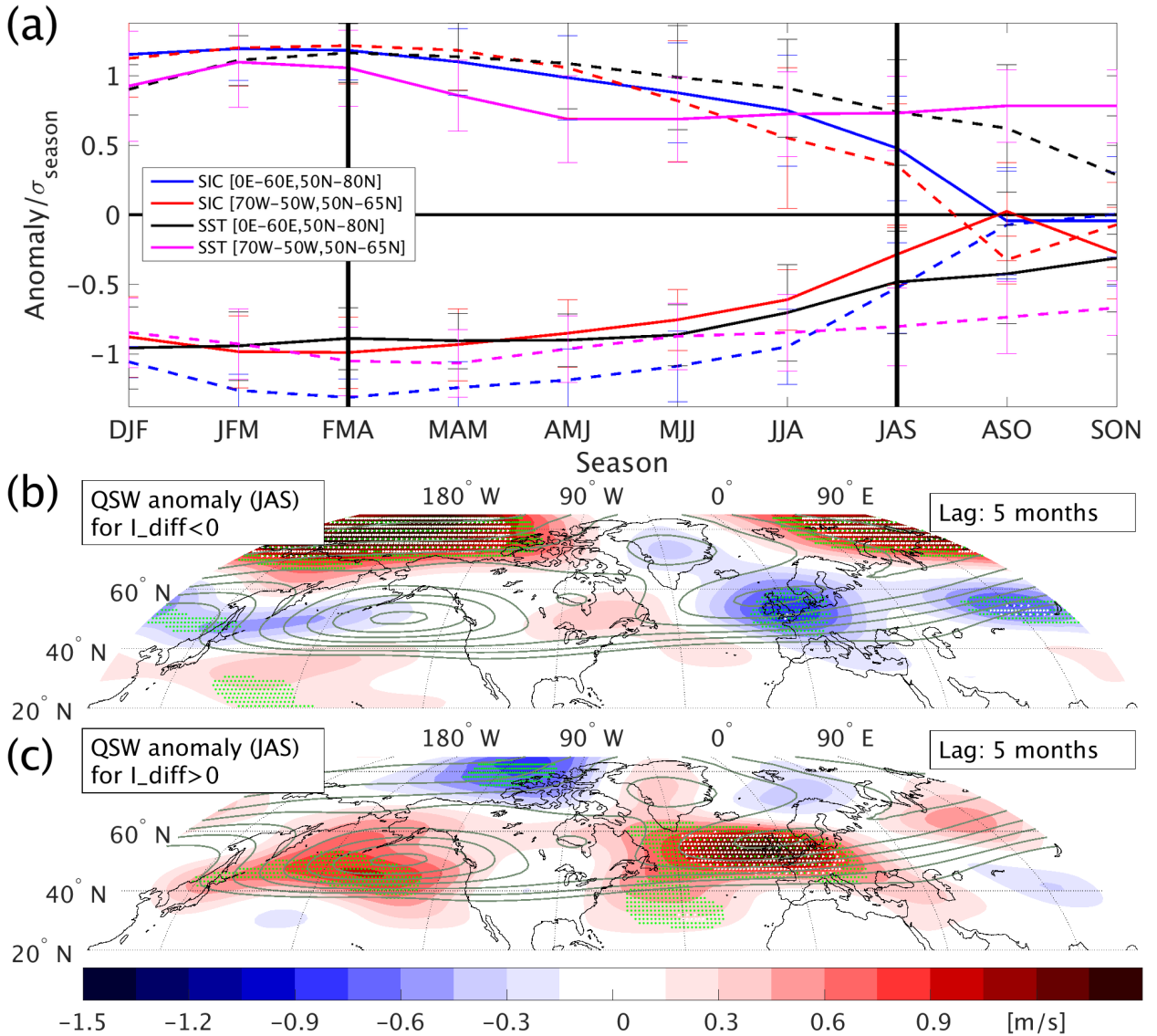
599 **Fig. 3.** Panel a shows SST and SIC persistence for a composite of the 8 years with the strongest
 600 positive and negative I_{diff} values in FMA. I_{diff} represents the difference of SIC box averages
 601 between the Labrador Sea (70°W to 50°W, 50°N to 65°N) and Greenland-Barents Sea (0°E
 602 to 60°E, 50°N to 80°N). Blue and black lines show the averaged values of SST and SIC
 603 in the Greenland-Barents Sea; red and magenta lines show the averaged values of SSTSIC
 604 in the Labrador Sea. Values associated with positive (negative) values of I_{diff} are given by
 605 solid (dashed) lines. All values are seasonally detrended and normalized by the associated
 606 seasonal standard deviation. Panel b (panel c) shows the associated anomalous QSW am-
 607 plitudes in JAS for the same composite years with $I_{diff} < 0$ ($I_{diff} > 0$). Statistical significance
 608 above the 95th (99th) percentile is given by the green (white) dots. Mean QSW amplitudes
 609 are given by the contour lines, spaced every 0.75 m/s, starting at 7.5 m/s. 30



610 FIG. 1. **Panel (a)** shows the first MC mode for the lagged covariance matrix between extended Northern
 611 Hemisphere (20°S to 85°N) SSTSIC and extratropical Northern Hemisphere (30°N to 85°N) QSW anomalies.
 612 Shading represents covariance between associated anomalies, weighted by their respective seasonal standard
 613 deviation. Seasons for the SSTSIC fields are given in panel (a) on the x-axis and are represented by the initial
 614 letters of the associated months. For the seasonally averaged QSW amplitudes a lag of -6 to $+9$ months is ap-
 615 plied (given on the y-axis); positive lags therefore mean that the SSTSIC is leading QSW. [excluded (description
 616 of stat. sign. in the method section): Statistical significance is calculated by using a Monte Carlo approach,
 617 repeating the analysis 1000 times with the same seasons and lags, but randomly choosing years for the QSWs.]
 618 Green pluses (dots) show statistical significant covariances based on 95th (90th) percentile. Red dots show
 619 those instances when the MC mode is not separable from the following mode, following the rule of thumb of
 620 North et al. (1982). Additional contour lines represent correlations between one of two global pattern indices
 621 (Niño 3.4 in black and NAO in blue) and the lagged QSW MC mode.
 622 **Panel (b)** shows the associated latitude-longitude pattern for the box, marked by the white edges in panel (a), for
 623 NDJ SSTSIC and JFM QSW (lag of $+2$ months). Boundaries for the regions used in the MC analysis are given
 624 by the black dashed lines. Shading shows anomalies of SST. Gray solid (dashed) contour lines show positive
 625 (negative) anomalies of QSW amplitude, spaced every 0.5 m/s omitting the zero contour line. Magenta (positive
 626 values) and green (negative values) contour lines show anomalies in SIC, spaced every 0.04 omitting the zero
 627 contour line. All variables shown are calculated via the projection of this variable onto the timeseries of the first
 628 principal component.



629 FIG. 2. First MC mode between Atlantic (80°W to 50°E and 20°N to 85°N) SSTSIC and extratropical
 630 Northern Hemisphere (30°N to 85°N) lagged QSW anomalies (boundaries of these regions shown by black
 631 dashed lines in panel (b) and (c)). Panel (b) and (c) show the associated latitude-longitude pattern for the boxes,
 632 marked by the white edges in panel (a), for JFM SSTSIC and DJF QSW (panel b, lag -1 month) and for FMA
 633 SSTSIC and JAS QSW (panel c, lag +5 months). Gray solid (dashed) contour lines show positive (negative)
 634 anomalies of QSW amplitude, spaced every 0.25 m/s omitting the zero contour line. Description for all other
 635 shadings, contours, etc. are the same as in Fig. 1.



636 FIG. 3. Panel a shows SST and SIC persistence for a composite of the 8 years with the strongest positive and
 637 negative I_{diff} values in FMA. I_{diff} represents the difference of SIC box averages between the Labrador Sea (70°W
 638 to 50°W, 50°N to 65°N) and Greenland-Barents Sea (0°E to 60°E, 50°N to 80°N). Blue and black lines show
 639 the averaged values of SST and SIC in the Greenland-Barents Sea; red and magenta lines show the averaged
 640 values of SST and SIC in the Labrador Sea. Values associated with positive (negative) values of I_{diff} are given by
 641 solid (dashed) lines. All values are seasonally detrended and normalized by the associated seasonal standard
 642 deviation. Panel b (panel c) shows the associated anomalous QSW amplitudes in JAS for the same composite
 643 years with $I_{\text{diff}} < 0$ ($I_{\text{diff}} > 0$). Statistical significance above the 95th (99th) percentile is given by the green (white)
 644 dots. Mean QSW amplitudes are given by the contour lines, spaced every 0.75 m/s, starting at 7.5 m/s.